Maria Sklodowska-Curie Actions (MSCA)
Innovative Training Networks (ITN)
H2020-MSCA-ITN-2018
Grant number 813137

Project number 813137

URBASIS-EU
New challenges for Urban Engineering Seismology

DELIVERABLE

Work Package: WP1
Number: D1.2 – Ground-motion Stochastic Simulations in Europe – Parameters Calibration from Spectral Decomposition Approach

Authors:	**Yen, Ming-Hsuan**	(GFZ)
Co-authors:	Cotton, Fabrice	(GFZ)
	Bindi, Dino	(GFZ)
Reviewer	Edwards, Ben	(UoL)

Approval	Management Board
Status	Final Version
Dissemination level	Public
Delivery deadline	31.10.2021
Submission date	01.02.2022
Intranet path	https://urbasis-eu.osug.fr/Scientific-Reports-157

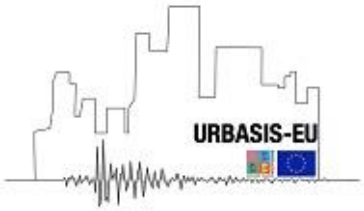

Index

1. **Introduction**
2. **Methodology**
   2.1 EXSIM - A Stochastic Extended Finite-Fault Ground-Motion Simulation Algorithm
   2.2 Spectral decomposition approach (General Inversion Technique, GIT)
3. **Data description**
4. **Outcomings from the GIT**
   4.1 Attenuation – Regionalized attenuation models in region A and B
   4.2 Site amplification – Joint datasets from both regions for isolating site and source terms
   4.3 Source spectra – Scaling relationship and spatial variation of stress drops
5. **Discussion and Conclusion**
6. **References**

D1.2: Ground-motion stochastic simulations in Europe – Parameter Calibration using a Spectral Decomposition Approach

Abstract

A spectral decomposition of the Fourier amplitude spectra is applied to determine the source parameters of earthquakes that have occurred in central-southern Europe. Using the event catalog from the International Seismic Centre (ISC), waveforms recorded in the target area since the late '90s have been downloaded from the European Integrated Data Archive (EIDA). A non-parametric decomposition approach is applied to isolate source, propagation and site contributions, which introduce a regionalization for the attenuation model into two spatial domains. For each domain, a spectral attenuation with hypocentral distance model is simultaneously determined in a tabular form and used to remove regional specific propagation effects from the spectra of recordings. Once isolated from local site effects, the obtained source spectra are fitted to a standard ω^2-model to determine the seismic moment and the corner frequency of each earthquake, which in turn are used to compute the stress drop considering a circular rupture model with uniform stress drop. In the report, we suggest to incorporate the resulting parameters from the inversion such as regional attenuation, site amplification and source parameters to the ground motion stochastic algorithm for the predicted ground motions.

1. Introduction

Ground-motion stochastic simulation is widely used to predict ground motions to develop ground-motion prediction equations (GMPEs) as an alternative to empirical methods for regions in which recordings from potentially damaging earthquakes are limited (Atkinson and Boore, 1995, 2006; Campbell, 2003; Pezeshk et al., 2011; Atkinson et al., 2014). It is particularly useful for simulating ground motions at high frequency of most interest to engineers (f>0.1Hz). One of the essential characteristics of the method is that it splits the various factors affecting ground motions (source, path, and site) into simple functional forms (Boore, 2003). Therefore, the factors can be adjusted with respect to regional conditions to obtain more realistic predicted ground motions.

In this study, we compute a spectral decomposition approach to determine the source, path, and site terms in central-southern Europe. We split the approach into two steps: 1) obtaining the regional attenuation functions by non-parametrical approach, and 2) jointing the Fourier amplitude spectra (FAS) corrected by regional attenuation functions separately in our two regions (northern and southern Europe). The parametric attenuations obtained by fitting the non-parametric attenuation functions and corrected the geometrical spreading are also determined for future implementation in the stochastic simulation method.

After the FAS have been corrected for regional attenuations, the site responses and source spectra can be obtained. The obtained source spectra are fitted to a standard ω^2-model to determine the seismic moment and the corner frequency of each earthquake, which in turn are used to compute the stress drop considering a circular rupture model with uniform stress drop.

The waveforms recorded in the target area since the late '90s have been downloaded from the European Integrated Data Archive (EIDA) within the tool, stream2segment (Zaccarelli et al., 2019), by using the event catalog from the International Seismic Centre (ISC). It is noted that the datasets are systemically downloaded by the stream2segment (Zaccarelli et al., 2019) from the continuous stream and the segments are 4 minutes of signal for all magnitudes. Some datasets would therefore be noise or contain artificial error or instrument error. Since high-quality data are required for the General Inversion Technique (GIT), quality control and preprocessing are applied.

2. Methodology

2.1 EXSIM – A Stochastic Extended Finite-Fault Ground-Motion Simulation Algorithm

The stochastic simulation method is a simple and powerful tool for simulating ground motions which is to combine parametric or functional descriptions of the ground motion's amplitude spectrum with a random phase spectrum modified by duration of motion and earthquake magnitude. The essential ingredient for the stochastic method is the spectrum of the ground motion—this is where the physics of the earthquake process and wave propagation are contained, usually split into the form of simple equations. The spectrum of motion is contributed from earthquake source, path, and site terms. The source term can be modeled as either a point source (Brune, 1970; Atkinson and Silva, 2000; Boore et al., 2014) or a finite source.

EXSIM is an open-source stochastic finite-source simulation algorithm which generates time series of ground motion for earthquakes (Motazedian and Atkinson, 2005; Boore, 2009; Liu et al., 2012; Boore et al., 2014). To consider the finite-fault effects (e.g., faulting geometry, distributed rupture, and rupture inhomogeneity) in ground-motion modeling, Hartzell (1978) proposed subdividing the fault surface of an earthquake into a grid of sub-sources, each of which could be treated as a point source. The contributions to ground motion can be summed at the observation site, over all of the sub-sources comprising the fault, considering proper delays of sub-sources due to rupture propagation. In EXSIM, time series from the sub-sources are modelled using the point-source stochastic model and popularized by the Stochastic-Method SIMulation (SMSIM) (Boore, 2003).

The stochastic point-source model assumes that the source process is concentrated at a point and that the acceleration time series radiated to a site carries deterministic and random aspects of ground-motion shaking. The deterministic aspects are specified by the average Fourier spectrum, given as a function of magnitude, distance and site characteristics. The stochastic aspects are treated

by modeling the motions as Gaussian noise with the specified underlying spectrum. The underlying deterministic spectrum is a multiplication of a source term (e.g., Brune, 1970) (Fourier spectrum at the source defined by seismic moment and stress parameter), a path term (anelastic attenuation and geometrical spreading), and a site term (crustal amplification and near-surface attenuation).

EXSIM uses the concept of dynamic corner frequency (Motazedian and Atkinson, 2005) in which the rupture begins with a high corner frequency and progresses to lower corner frequencies as the ruptured area grows. This makes the simulation results relatively insensitive to sub-source size. The duration of motion for each sub-source comes from the source duration plus the path duration. Finally, the time series from the sub-sources are summed in the time domain with a normalization factor, with appropriate time delays for propagation of the rupture front. This would result into a total seismic signal at a site of interest.

2.2 Spectral decomposition approach (Generalized Inversion Technique, GIT)

In order to calibrate the input parameters required to compute an average Fourier spectrum using stochastic simulation techniques, we perform a decomposition of the Fourier amplitude spectra into source, propagation and site terms considering a large data set compiled for the study area. The generalized inversion technique (GIT) (Castro et al.,1990) is well-known method to derive frequency-dependent attenuation characteristics as well as source and site spectra. In order to determinate the attenuation model, site amplification and source spectra from observed S-wave Fourier amplitude spectra, we apply the non-parametric approach introduced by Castro et al. (1990). The average Fourier amplitude spectra in this study is the geometrical mean of the two-horizontal component (EW and NS). The Fourier amplitude spectra of ground motion can be written as

$$U_{ij}(f, r_{ij}, M_i) = S_i(f, M_i) * A(f, r_{ij}) * Z_j(f) \quad (1)$$

where $U_{ij}(f, r_{ij}, M_i)$ is the observed Fourier amplitude spectra at the jth station from the ith earthquake with magnitude M_i; r_{ij} is the hypocentral distance; $S_i(f, M_i)$ represents the source spectrum of the ith earthquake; $A(f, r_{ij})$ stands for the attenuation along the travel path, and $Z_j(f)$ is the site response function of the jth station with unaccounted of instrument responses. Taking the logarithm of eq. (1) turns into a linear problem, the equation can be written as

$$log_{10}U_{ij}(f, r_{ij}) = log_{10}S_i(f) + log_{10}A(f, r_{ij}) + log_{10}Z_j(f) \quad (2)$$

In this study, we follow the non-parametric approach to avoid the assumption of simple parameterizations (e.g., monotonic decreasing function of distance) to describe the seismic attenuation and the source spectra. Here, we split the inversion into two steps: first, we determine the attenuation model introducing a two domains regionalization. The attenuation for each region is simultaneously determined by discretizing the distance range into a given number of intervals and determining the frequency-dependent attenuation value for each distance bin. For each frequency, the attenuation values are smoothed by requiring their second derivative to be small (Castro et al., 1990). The equation can be written as

$$log_{10}U_{ij}(f, r_{ij}) = log_{10}A^{k}(f, r_{ij}) + log_{10}R_{ij}(f) \quad (3)$$

where k=1,2 indicates the regionalization of the attenuation model.

After the regional attenuation functions have been determined, a subsequent inversion allows separating source and site effects:

$$log_{10}R_{ij}(f) = log_{10}S_{i}(f) + log_{10}Z_{j}(f) \quad (4)$$

Herein, $log_{10}R_{ij}(f) = log_{10}U_{ij}(f, r_{ij}) - log_{10}A^{k}(f, r_{ij})$ are the residual spectral amplitudes after correcting the attenuation functions. In this study, we discuss on the attenuation characteristics $A^{k}(f, r_{ij})$ resulting from the first step, and the site amplification and source spectra obtained from the second inversion step.

The second step is that we set up the amplification at the reference site to 1 for frequencies below 10 Hz and to $e^{-\pi k_0(f-10)}$, with k_0= 0.007s, above 10 Hz. Therefore, the site relative amplifications at all considered stations are estimated with respect to the applied reference site condition. It is worth to remember that the trade-off between source and site terms also links the source spectra to this assumption.

3. Data description

The data download process to our database is guided by a seismic event catalog which is the event webservice of the International Seismological Center, ISC. The largest time span of the data considered is from January 1st, 1990 to May 31st, 2020 and the maximum hypocentral depth was set to 60 km to include the crustal events. To ensure the events with magnitudes (M2-7) from diverse hypocentral distances are complete recorded in the target windows, the segments are 4 minutes long starting 1 minute before the theoretical P-wave arrival time (computed considering the AK135 global

velocity model). Since the window is large and it would contain the multiple events, the multiple event detection is applied during the preprocess. The selected segments are with the three components of motion from HH, HN, HL, HG, EH channels. The channel names are following the SEED convention, that is, high sampling rate channels from broad band (HH), short period (EH) and strong motion instruments (HN but also HL and HG). Our database hosts about 52 million segments in total from 178,000 earthquakes recorded by 4,771 stations belonging to 118 either temporary or permanent networks. It is noted that the datasets are systemically downloaded by the stream2segment (Zaccarelli et al., 2019).

Since the high-quality data requirement of the GIT, the quality control and preprocessing are applied. The datasets are preprocessed by the following the main steps to have the first filtering (Figure 1):

1) check for possible clipped signal by simply comparing the maximum digital count in the trace with the fraction (80%) of the full scale (FS) = (2^{24-1}) of a 24-bit digitizer;

2) band-pass filter the trace using a zero-phase, 2-poles, Butterworth filter with high pass corner frequency f_H being magnitude dependent and the low pass corner frequency fixed to 90% of the Nyquist. Corner frequency f_H was set to 0.08 Hz for magnitude above 6; to 0.3 for magnitudes between 3 and 6; and to 0.5 Hz for events smaller or equal to 3;

3) the instrumental response is removed in the spectral domain setting the water level regularization to 60 dB, and converted to the acceleration and restituted in the acceleration; the signal window is defined as the interval between the 2.5% and 97.5% percentile of the cumulative squared acceleration computed from the estimated P-wave arrival.

During preprocessing, quality control of the segments is applied to filter out the potential noise at the first stage. We computed the simple multiple event detection (Cauzzi et al., 2016) and signal-to-noise ratio (SNR) to drop segments with the potential multiple-event signal and segments which SNR is lower than 20. The window with multiple events is discarded based on automatic procedure based on the analysis of the second derivative of the cumulative squared acceleration. The SNR is computed over different frequency ranges: [fmin,0.5], [0.5, 20], [fmin, fmax] Hz, and segments with SNR [0.5-20 Hz] smaller than 20 are no further processed. The surviving datasets are shown in Figure 2. We split the dataset into two regions for the regionalization of the attenuation model, which are located in A) mainly Germany and B) mainly Italy. The magnitudes of the datasets are from 2 with many types of magnitude (M_L, M_s, M_b etc.). We discard segments corresponding to events with magnitude lower than 3 recorded at distances larger than 80 km.

The second step of the data selection is the outlier detection which is a modified Z-score method applied to the median absolute deviation of residuals. The residuals are the respect to predictions from Ground Motion Prediction Equations (GMPEs) considering the PGV and PGA for

Europe and Middle East (Bindi et al., 2014) to detect the presence of outliers. The threshold is according to Iglewicz and Hoaglin (1993) that suggested the Z-score for the presence of outliers was greater than 3.5 or lower than -3.5.

For the spectral decomposition approach, the Fourier amplitude spectrum (FAS) is computed by the vector sum of two horizontal components, which is independent on the sensor rotation. The considered frequency band is from 0.5 to 20 Hz. The geometric mean of the peak ground velocity (PGV) and acceleration (PGA), as generally implemented in ground motion prediction equations, is also computed by selecting segments with minimum SNR over the two horizontal components larger than the applied threshold.

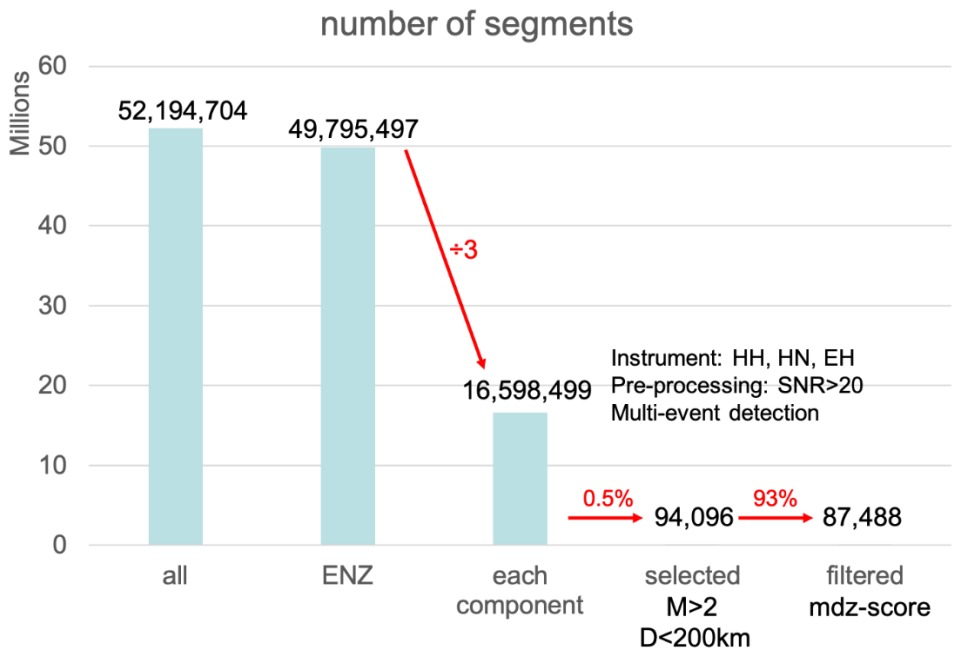

Figure 1. The dataset reduction by each processing and filtering steps.

(a)

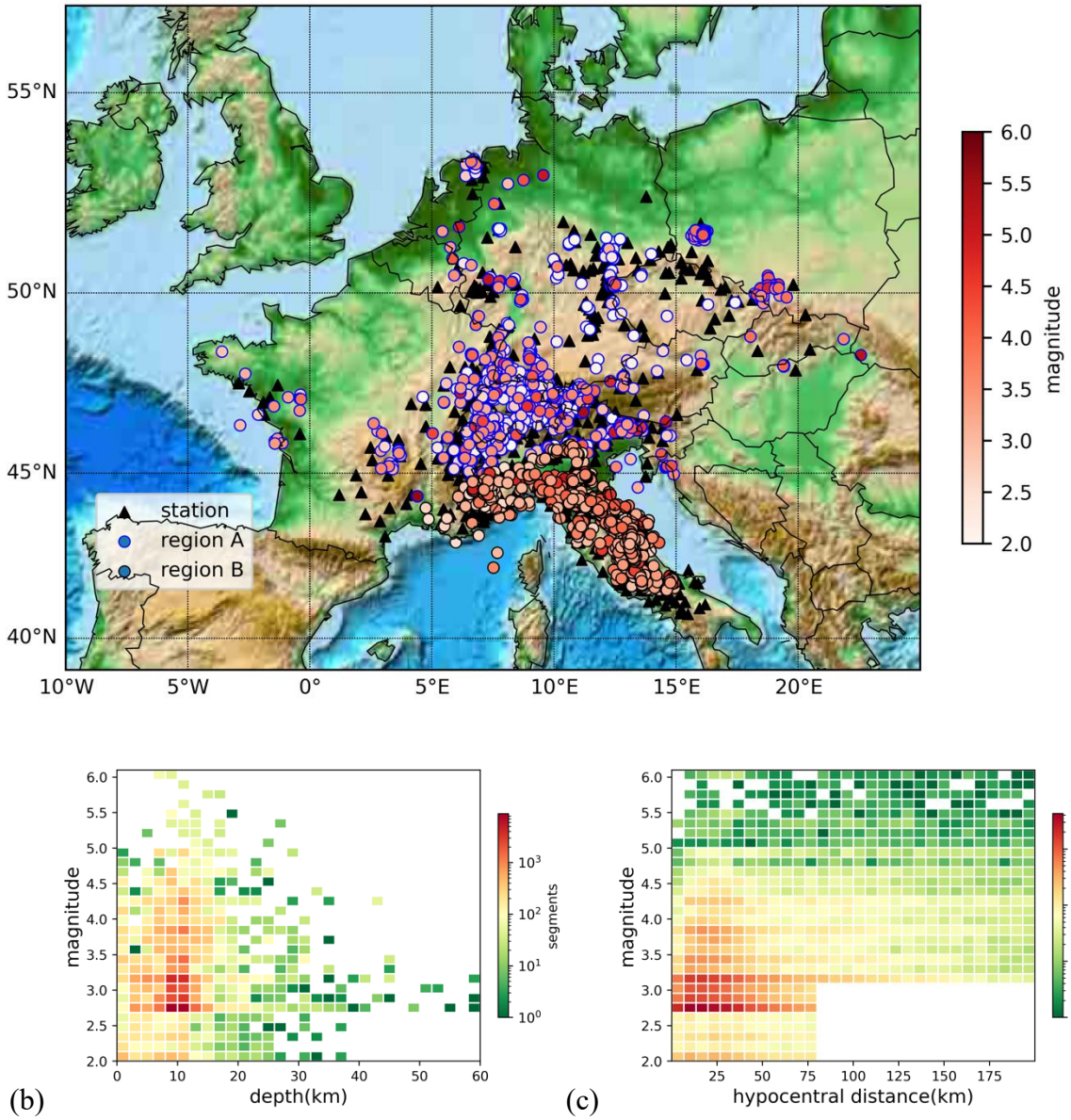

Figure 2. (a) The distribution of stations and events in our study. Earthquakes magnitude as function of (a) depth and (b) hypocentral distance.

4. Outcomings from the GIT

4.1 Attenuation – Regionalized attenuation models in region A and B

To assess the stability of the inversion results, we perform 100 bootstrap inversions at each frequency point following the procedure detailed in Parolai et al. (2000, 2004). The applied GIT inversion is two-step non-parametric approach which isolates the source, site, and path functions directly that we take only the attenuation models in the first step for later correction to isolate source and site terms, and in the second step we correct FAS by the obtained attenuation models first and separate the source and site terms. We constrain $A(f, r_{ij})$ to a smooth function of distance as well as $A(f, r_0) = 1$, with r_0 is equal to 10 km. The distance range from 0 to 200 km is subdivided into distance bins of 5 km wide to determine the attenuation functions. Previous GIT studies performed in Japan (Oth et al., 2011) showed that the resulting attenuation functions are completely independent of the reference site condition and the changes in the site constraint result in purely anticorrelated changes in the source contributions. We also observed this phenomenon in our datasets. It points out that to obtain stable results for seismic attenuation is possible even if no appropriate reference site or source is available. Therefore, the constraint of the site response function at each frequency point was set to the average site response of all stations for determining the attenuation models in this case.

In this first step of the spectral decomposition, we capture the regionalized attenuation model of two regions, respectively. The attenuation functions for all frequency points between 0.5 and 20 Hz show in Figure 2a. The attenuation functions in region A almost decay the same as 1/R function up to 60 km. At large distances, the attenuation functions attenuate faster than 1/R curve at the frequency larger than 10 Hz. The attenuation functions in region B decay the same for the entire frequency range at distance up to 50 km. At the distance larger than 50 km, the attenuation functions at high frequency attenuate faster. It points out that in the southern Europe (region B) has a stronger attenuation than the northern Europe (region A), especially at high frequency.

Subsequent applications for the ground motion stochastic simulation could benefit from a parametrization of the attenuation model in terms of geometrical spreading and quality factor (anelastic attenuation). In order to provide a first sight for the application to stochastic simulations, we perform a preliminary parametrization by considering a simple geometrical spreading given by R_0/R for both of regions. The usage of more complex geometrical spreading function as considered by Bora et al. (2015) will be considered in future works (e.g., piece-wise linear geometrical spreading models with different distance-hinges, and for Q(f) models with different frequency-hinges).

The obtained non-parametric attenuation functions can be described in terms of geometrical spreading and apparent shear wave quality factor (anelastic attenuation) by the following relation (Boore, 1983):

$$A(f,R) = G(R)exp\left[\frac{-\pi f(R-R_0)}{Q(f)V_S}\right],$$

where $G(R)$ is the geometrical spreading function, R is the hypocentral distance in km, R_0 is the reference distance for the fitting, $Q(f)$ is the apparent shear wave quality factor and V_S is the shear wave velocity. We first simply considered that the geometrical spreading is R_0/R for both of regions to get the first sight of the quality factor in this case. This model is applied to correct the obtained attenuation functions and to extract the frequency-dependent attenuation model including the S-wave quality factor contribution. Under the assumption that the geometrical spreading is frequency independent, the adopted model could be applied to all frequencies to obtain the apparent quality factor.

The frequency-dependent quality factor, $Q(f)$, is determined from the slop of a least-square regression to $logA(f,r) - logG(r)$ versus distance. Finally, a power function of the form $Q(f) = Q_0 f^N$ is fitted to the estimated $Q(f)$ values to determine Q_0 and N through least-squares inversion as well. It is noted that the obtained $Q(f)$ are dependent on the geometrical spreading models considered here. The values of $Q(f)$ for all 44 frequencies and the least-squares fit of the power function in two regions are shown in Figure 4. The values of frequency-dependent quality factors are determined and obtained at all 44 frequencies for both regions:

$Q(f) = 216.18f^{0.61}$ for region A,
$Q(f) = 113.87f^{0.65}$ for region B.

The vertical error bars in Figure 4 indicate the regression error of fitting from the linear regression performed at each frequency. The obtained $Q(f)$ in two regions follows a roughly linear trend with frequency, yet the regression error at low frequency are larger and is more scatter in region A. The tendencies of the quality factor at high frequencies (>10Hz) are becoming less frequency dependent in both regions.

However, the obtained $Q(f)$ are dependent on the geometrical spreading models considered. The assumption of the geometrical spreading is simply set as 1/R in this case. Theoretically, geometrical spreading is equal to 1/R at near distances (<50 to 100km) for an isotropic and homogenous whole space (Bora et al., 2017). However, many studies found the geometrical spreading should be a complex function of distance (Atkinson and Mereu, 1992; Edwards et al. 2008; Atkinson and Boore, 2011). Therefore, for our future work we will consider the complex geometrical spreading function derived in Bora et al. (2015) in order to limit potential trade-off and bias.

(a) (b)

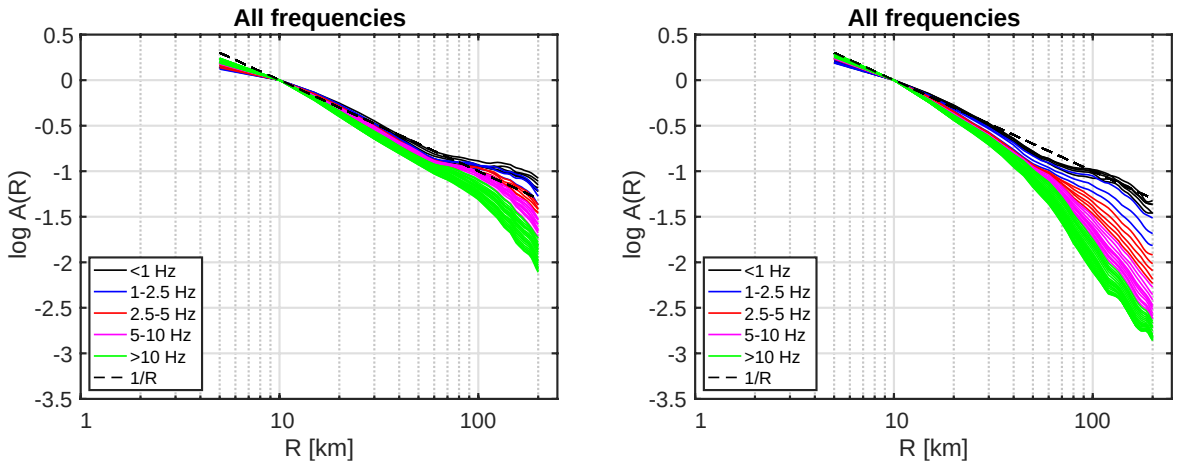

Figure 3. Non-parametric attenuation functions versus hypocentral distance for all 40 frequencies in (a) region A and (b) region B. The R^{-1} (black dash line) curve is displayed for comparison. Note that $logA(f, r_0) = 0$ at the reference distance r_0 =10 km.

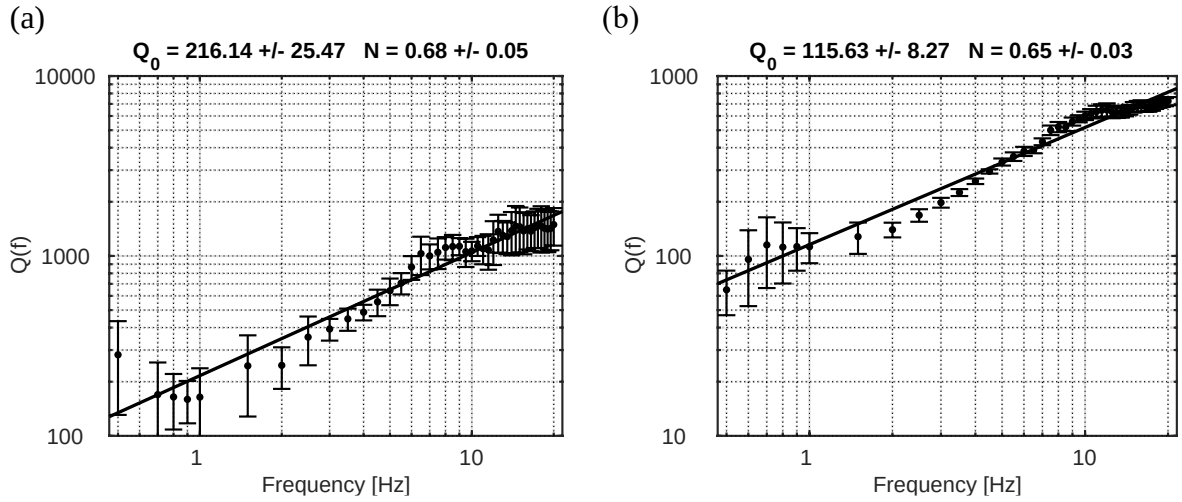

Figure 4. The solid black line indicates the obtained $Q(f)$ model from the analysis of the attenuation functions from GIT inversion for single decay geometrical spreading in (a) region A and (b) region B. The individual Q values derived at each given frequency are denoted by dots and error bars.

4.2 Site amplification – Joint datasets from both regions for isolating site and source terms

In order to determine site response functions and source spectra relative to the same reference condition for both regions, we corrected the FASs by the non-parametric attenuation models from the first step non-parametric approach for each region and joint datasets from two different regions to separate the site response and source spectra terms. In order to make the resulting source terms comparable in both regions, the constraint of the reference site is set to the station CH.LLS, which is the reference site in the network CH managed by Swiss seismological service (SED). The site amplification at the reference station CH.LLS (station Linth-Limmern) is constrained to a function equal to 1 for frequencies below 10 Hz with κ_0 = 0.007 s (Pilz et al., 2019). The reference site response is shown in Figure 5 (CH.LLS). We selected the stations and events which are more than 3 recordings per station and per event for the source and site terms isolation.

Examples of the site amplifications with one standard deviation at the broadband instruments are shown in Figure 5. It is noted that all site amplification functions are relative to the reference site, CH.LLS, which site response is flat as Figure 5. The standard deviations of the site amplifications at example stations in Figure 5 get higher when the considered recordings at the stations are fewer.

Figure 6 shows the site amplification of the different instruments at the same stations. At some stations the site amplifications are quite different at different channels. Whereas the availability of different instruments co-located at the same site can be exploited to enlarge the frequency range used for the site effect evaluation (e.g., low-frequency teleseismic events recorded by broad-band channels and high-frequency close events recorded by accelerometric channels), it can be also used to detect potential outliers due to metadata inconsistencies. Moreover, site amplification estimation depends on good azimuthal and distance coverage, reliable site responses can be obtained only when earthquakes are distributed around the station in all directions at difference distances (Lermo and Chavez-Garcia, 1993; Parolai et al., 2004). Future works will be devoted to investigate these inconsistencies and to classify the reliability of the GIT site terms in representing local site amplification effects.

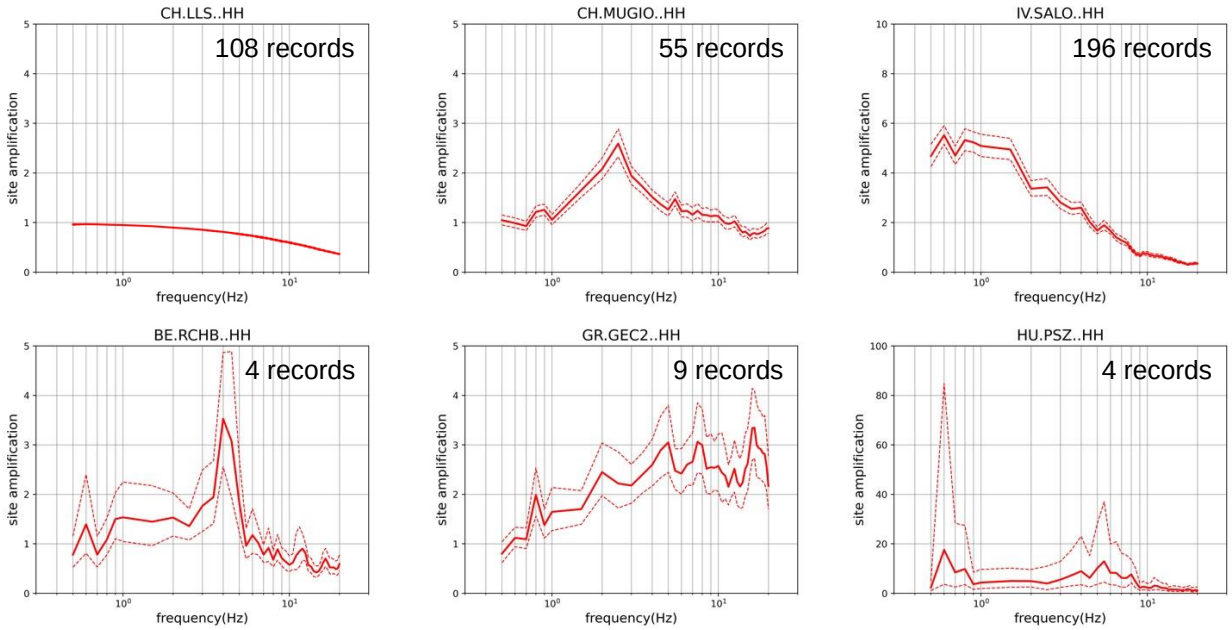

Figure 5. Site response functions in linear scale. Dash lines indicate one standard deviation from 100 bootstrap analysis.

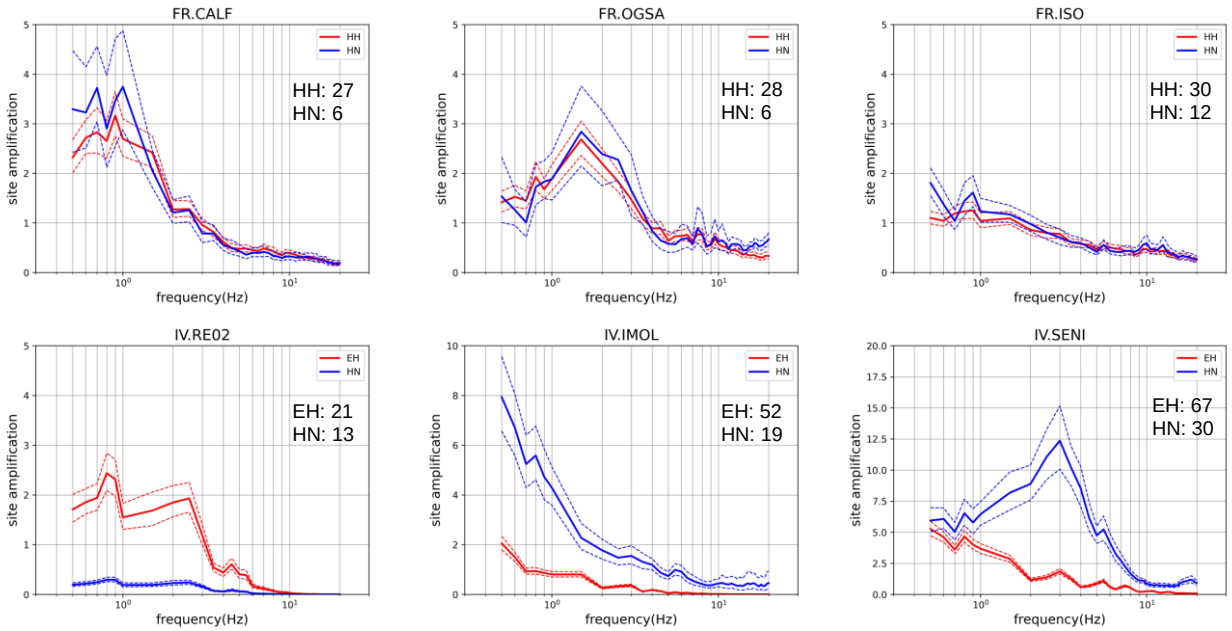

Figure 6. Site response functions in linear scale. Dash lines indicate one standard deviation from 100 bootstrap analysis. The numbers for different channels (HH, HN, EH) indicate the numbers of the recordings.

4.3 Source spectra – Scaling relationship and spatial variation of stress drops

After the attenuation-corrected spectra are separated into their source and site contributions, the obtained source spectra can determine the source parameters by fitting the ω^2-model (Brune, 1970, 1971). For the further application of the stochastic simulation, the source term we suggest to consider the distribution of the resulting stress drops which determined from the ω^2-model fitting. In this report, we show the preliminary scaling relationship and spatial variation of stress drops to first sight the possibility of the application for the stochastic simulation.

Figure 7 shows all source spectra at 10 km reference distance. Source spectral fits with the ω^2-model (Brune, 1970, 1971) were carried out to determine corner frequency f_C and seismic moment M_0 (respectively moment magnitude M_W), using nonlinear least squares (Oth et al., 2011):

$$S(f) = (2\pi f)^2 \frac{R^{\theta\emptyset} F}{4\pi\rho {V_S}^3 R_0} \dot{M}(f), with \dot{M}(f) = \frac{M_0}{1 + (f/f_C)^2}$$

Where $S(f)$ represents the acceleration source spectrum at the reference distance R_0 = 10 km. $\dot{M}(f)$denotes the moment-rate spectrum, $R^{\theta\emptyset}$is the average radiation pattern of S-waves set to 0.55 (Boore and Boatwright, 1984), F=2 is the free surface factor, and ρ=2.7 g/cm^3 is the density and V_S= 3.3 km/s is the shear-wave velocity near the source. Stress drop $\Delta\sigma$ was computed with the obtained corner frequency and moment magnitude by the following equation (Eshelby, 1957):

$$\Delta\sigma = \frac{7M_o}{16r^3}$$

where the rupture radius is given by

$$r = \frac{2.34V_S}{2\pi f_C}$$

In Figure 7, the source spectra have lower amplitude of the event M4-5 than that of the event M3-4, which might be the effect of the attenuation and site response corrections. Figure 8a shows the corner frequency against the inverted seismic moment. The relationship expected for a self-similar behavior should show a -1/3 slope and the obtained data shows a slope which is not far from that theoretical self-similar behavior. The scaling relationship of stress drop with earthquake size is still a controversial issue in seismology and earthquake source mechanics. Figure 8b shows the clear scaling relationship of the stress drops with the moment magnitude that the larger earthquakes have larger stress-drops. The distribution of stress drops in two regions are shown in Figure 8c. The resulting stress drops are mainly distributed in the range of 0.01-10 MPa in region A and 0.1-100 MPa in region

B. The spatial variation of the stress drops shows in Figure 9. The stress drops have a sharp difference between two regions. The spatial variation of the stress drop values has a strong regional variation. Since we derived the attenuation models by performing separate decomposition in the two regions, the strong spatial variation of the stress drop might be a trade-off effect, suggesting that the effect of introducing the regionalization should be further checked.

. In Figure 8a, the inverted magnitudes (GIT_Mw) is compared to the magnitude from ISC retrieved during the events download. The inverted magnitudes (GIT_Mw) are lower than ISC magnitude for the large earthquakes and larger than ISC magnitude for some small earthquakes (M2-3). For fitting the ω^2-model, an unambiguous fit of moment and corner frequency is not possible for large events. In addition, whereas ISC is providing a large variety of magnitudes as provided by different observatories or re-computed by ISC, the magnitude retrieved during the event-download can be of different type (m_b, M_s, M_L…), and no action in this work has been taken to harmonize them. For future applications in the framework of hazard assessment, the consistency among the magnitudes derived in this study with those listed in the seismic catalogs compiled for the hazard assessment is of relevance. Therefore, in a future step, we will consider magnitude from EMEC catalog (Grünthal et al., 2009) as a reference to constrain the low-frequency plateau of the non-parametric source spectra.

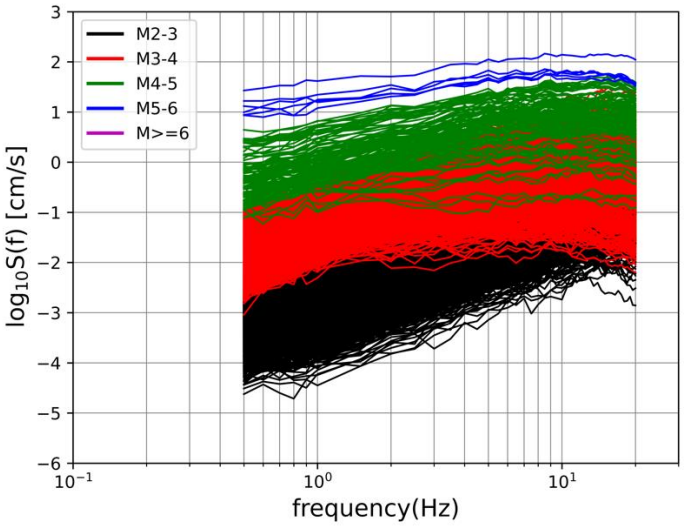

Figure 7. Source spectra after the attenuations and site responses correction. Magnitude of the source spectra are the magnitude derived in this study.

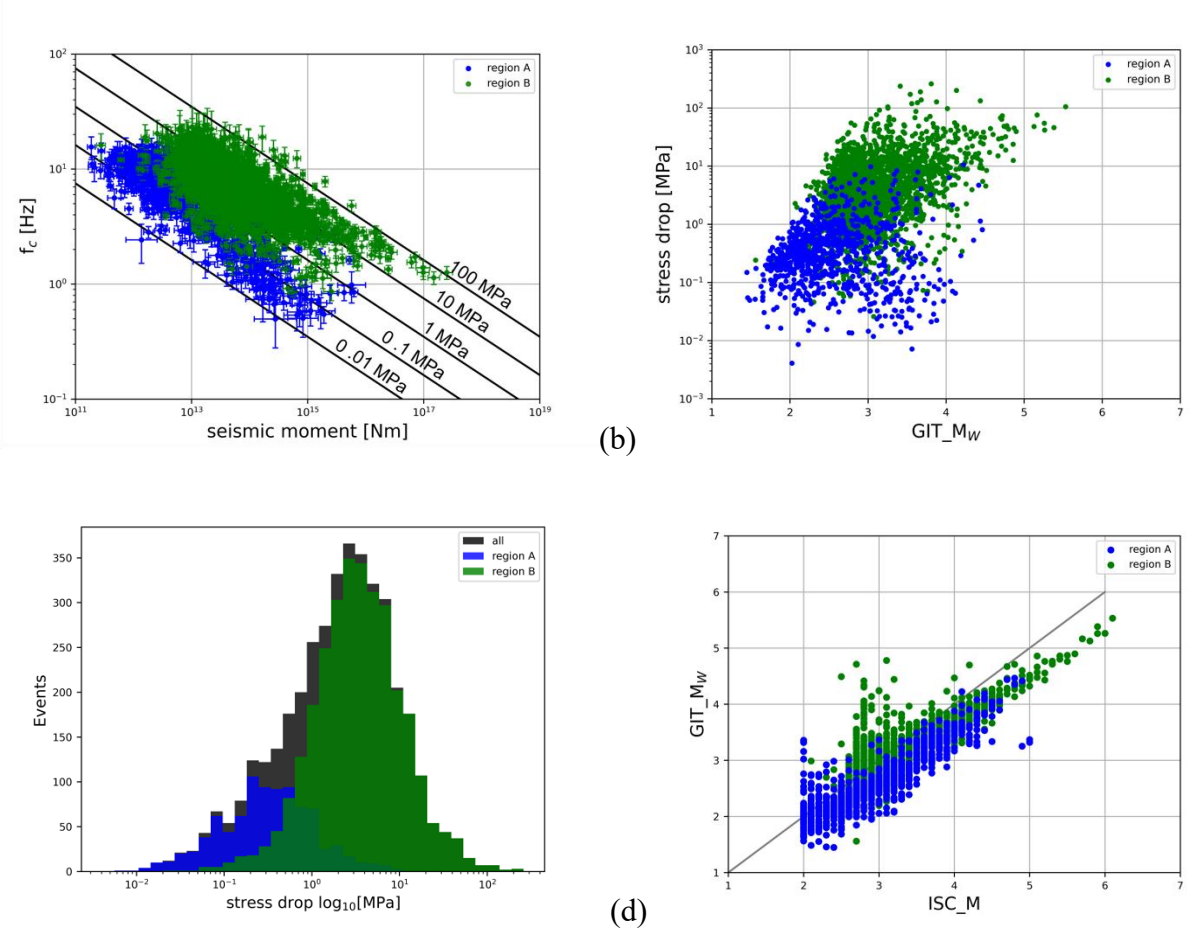

(a) (b)

(c) (d)

Figure 8. (a) Scaling results of the corner frequency against the seismic moment. (b) Stress drops scaling with magnitude from database. (c) Scaling of the inverted magnitude against the magnitude from database. (d) The distribution of the stress drops in two different regions. Blue indicates the results of region A. Green indicates the results of region B.

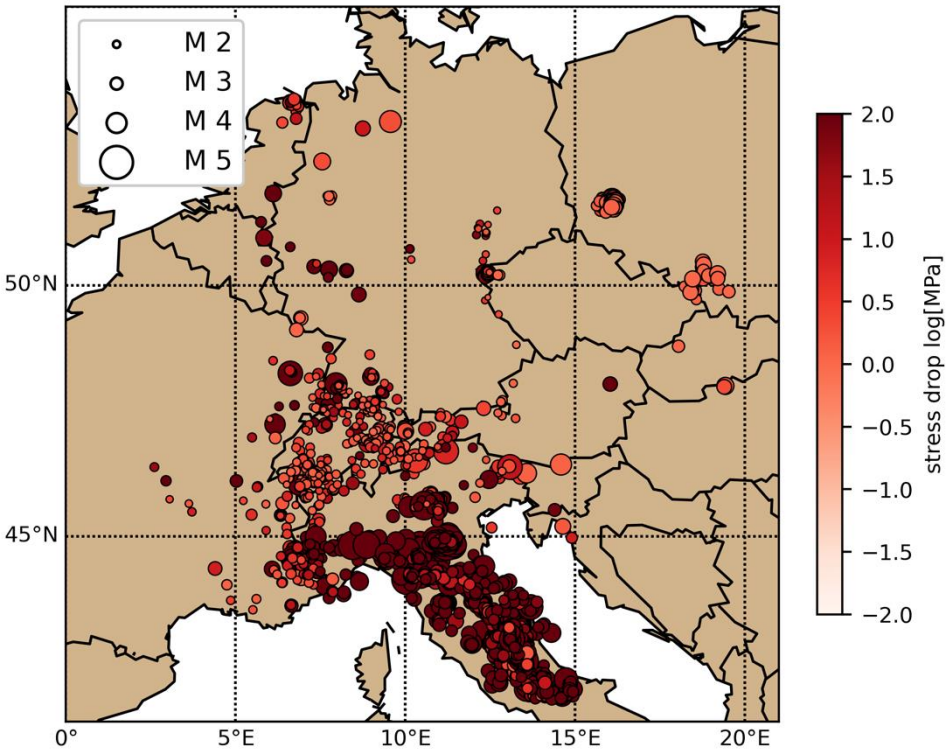

Figure 9. Regional variation of the stress drops. Color represents the stress drops. The size of circles indicates the earthquake magnitudes.

5. Discussion and Conclusion

The spectrum of the ground motion is the essential ingredient for the stochastic simulation which is the contribution of earthquake source, wave propagation, and site amplification. The assumptions for each term of the spectrum of the ground motion in the simulation are referred to the theoretical equations or scaling relationships in the world. However, the computations of the ground motion simulation in Europe require a proper models and scaling relationships in the area. In this study, we analyze about one hundred thousand recordings in Europe which provide a good opportunity to learn the source, path and site terms for the essential ingredient for the stochastic simulation.

For the path term, we proposed non-parameter regional attenuation models for two regions as region A (northern Europe) and region B (southern Europe). The models show that the attenuation is similar in both regions at short distance and stronger in the south (Italy) than in the north (central Europe) at large distance and high frequencies. The parametric attenuation models are also determined from the non-parametric attenuation models with simple assumption of the geometrical spreading which is the function, R_0/R for the first sight of the quality factors in two regions. According to several studies, the geometrical spreading should be considered different level of complexities of the parametric form to limit potential trade-off and bias. In our future work, the geometrical spreading function derived in Bora et al. (2015) would be consider to determine the quality factors in our next-step correction. (e.g., piece-wise linear models with different distance-hinges, and for Q(f) different frequency-hinges).

Resulting stress drops in this study shows a clear scaling related to earthquake magnitude, which is increasing with earthquake moment magnitude. The regional variation of stress drop shows that the stress drops in the south are in general larger than that in the north with sharp difference between two regions. However, the spatial variation of stress drop has a regional difference which might be the effect from the regional attenuation correction. It suggests that the effect of the regional attenuation correction should be further checked.

This report presented the analysis performed over a large data set to derive spectral models for central and southern Europe. Although several aspects need further investigations (e.g., role of the regionalization and possible trade-offs between source and attenuation terms; assessment of the consistency among the site terms derived at the same stations considering different instruments; compatibility of the low-source spectral values for target events with catalogs used for hazard assessment), the outcomes of this study show that the large availability of seismic data disseminated in a standardized way by EIDA can be used to constrain the distributions of seismic parameters involved in stochastic simulation of ground shaking (e.g.. Edwards and Fäh, 2013; Drouet and Cotton, 2015).

6. References

Atkinson, G. M., and D. M. Boore, 1995, Ground-motion relations for eastern North America, Bulletin of the Seismological Society of America, 85, no. 1, 17–30, doi: 10.1785/BSSA0850010017.

Atkinson, G. M., and D. M. Boore, 2011, Modifications to Existing Ground-Motion Prediction Equations in Light of New Data, Bulletin of the Seismological Society of America, 101, no. 3, 1121–1135, doi: 10.1785/0120100270.

Atkinson, G. M., and R. F. Mereu, 1992, The shape of ground motion attenuation curves in southeastern Canada, Bulletin of the Seismological Society of America, 82, no. 5, 2014–2031, doi: 10.1785/BSSA0820052014.

Atkinson, G. M., and W. Silva, 2000, Stochastic Modeling of California Ground Motions, Bulletin of the Seismological Society of America, 90, no. 2, 255–274, doi: 10.1785/0119990064.

Atkinson, G. M., J. J. Bommer, and N. A. Abrahamson, 2014, Alternative Approaches to Modeling Epistemic Uncertainty in Ground Motions in Probabilistic Seismic-Hazard Analysis, Seismological Research Letters, 85, no. 6, 1141–1144, doi: 10.1785/0220140120.

Bindi, D., M. Massa, L. Luzi, G. Ameri, F. Pacor, R. Puglia, and P. Augliera, 2014, Pan-European ground-motion prediction equations for the average horizontal component of PGA, PGV, and 5 %-damped PSA at spectral periods up to 3.0 s using the RESORCE dataset, Bull Earthquake Eng, 12, no. 1, 391–430, doi: 10.1007/s10518-013-9525-5.

Boore, D. M., 2003, Simulation of Ground Motion Using the Stochastic Method, Pure appl. geophys., 160, no. 3, 635–676, doi: 10.1007/PL00012553.

Boore, D. M., 2009, Comparing Stochastic Point-Source and Finite-Source Ground-Motion Simulations: SMSIM and EXSIM, Bulletin of the Seismological Society of America, 99, no. 6, 3202–3216, doi: 10.1785/0120090056.

Boore, D. M., and J. Boatwright, 1984, Average body-wave radiation coefficients, Bulletin of the Seismological Society of America, 74, no. 5, 1615–1621, doi: 10.1785/BSSA0740051615.

Boore, D. M., C. Di Alessandro, and N. A. Abrahamson, 2014, A Generalization of the Double-Corner-Frequency Source Spectral Model and Its Use in the SCEC BBP Validation Exercise, Bulletin of the Seismological Society of America, 104, no. 5, 2387–2398, doi: 10.1785/0120140138.

Bora, S. S., F. Cotton, F. Scherbaum, B. Edwards, and P. Traversa, 2017, Stochastic source, path and site attenuation parameters and associated variabilities for shallow crustal European earthquakes, Bull Earthquake Eng, 15, no. 11, 4531–4561, doi: 10.1007/s10518-017-0167-x.

Bora, S. S., F. Scherbaum, N. Kuehn, P. Stafford, and B. Edwards, 2015, Development of a Response Spectral Ground-Motion Prediction Equation (GMPE) for Seismic-Hazard Analysis from

Empirical Fourier Spectral and Duration Models, Bulletin of the Seismological Society of America, 105, no. 4, 2192–2218, doi: 10.1785/0120140297.

Brune, J. N., 1970, Tectonic stress and the spectra of seismic shear waves from earthquakes, Journal of Geophysical Research (1896-1977), 75, no. 26, 4997–5009, doi: 10.1029/JB075i026p04997.

Brune, J. N., 1971, Seismic sources, fault plane studies and tectonics, Eos, Transactions American Geophysical Union, 52, no. 5, IUGG 178-IUGG 187, doi: 10.1029/EO052i005pIU178.

Campbell, K. W., 2003, Prediction of Strong Ground Motion Using the Hybrid Empirical Method and Its Use in the Development of Ground-Motion (Attenuation) Relations in Eastern North America, 22.

Castro, R. R., J. G. Anderson, and S. K. Singh, 1990, Site response, attenuation and source spectra of S waves along the Guerrero, Mexico, subduction zone, Bulletin of the Seismological Society of America, 80, no. 6A, 1481–1503, doi: 10.1785/BSSA08006A1481.

Cauzzi, C, R. Sleeman, J. Clinton, J. D. Ballesta. O. Galanis, and P. Kästli, 2016, Introducing the European Rapid Raw Strong-Motion Database, Seismological Research Letters 87 (4): 977-986.

Drouet, S., and F. Cotton, 2015, Regional Stochastic GMPEs in Low-Seismicity Areas: Scaling and Aleatory-Variability Analysis Application to the French Alps. Bulletin of the Seismological Society of America, 105, 4, p. 1883-1902

Edwards B. and Fäh D., 2013, A stochastic ground-motion model for Switzerland. Bull Seismol Soc Am 103(1):78–98. doi:10.1785/0120110331

Edwards, B., A. Rietbrock, J. J. Bommer, and B. Baptie, 2008, The Acquisition of Source, Path, and Site Effects from Microearthquake Recordings Using Q Tomography: Application to the United Kingdom, Bulletin of the Seismological Society of America, 98, no. 4, 1915–1935, doi: 10.1785/0120070127.

Eshelby, J. D., and R. E. Peierls, 1957, The determination of the elastic field of an ellipsoidal inclusion, and related problems, Proceedings of the Royal Society of London. Series A. Mathematical and Physical Sciences, 241, no. 1226, 376–396, doi: 10.1098/rspa.1957.0133.

Grünthal, G., Wahlström, R. (2012) The European-Mediterranean earthquake catalogue (EMEC) for the last millennium. Journal of Seismology 16(3): 535-570

Hartzell, S. H., 1978, Earthquake aftershocks as Green's functions, Geophysical Research Letters, 5, no. 1, 1–4, doi: 10.1029/GL005i001p00001.

Iglewicz, B. and Hoaglin, D.C., 1993. How to detect and handle outliers (Vol. 16). Asq Press.

Lermo, J., and F. J. Chávez-García, 1993, Site effect evaluation using spectral ratios with only one station, Bulletin of the Seismological Society of America, 83, no. 5, 1574–1594, doi: 10.1785/BSSA0830051574.

Liu, T. J., G. M. Atkinson, H. P. Hong, and K. Assatourians, 2012, Intraevent Spatial Correlation Characteristics of Stochastic Finite-Fault Simulations, Bulletin of the Seismological Society of America, 102, no. 4, 1740–1747, doi: 10.1785/0120110266.

Motazedian, D., and G. M. Atkinson, 2005, Stochastic Finite-Fault Modeling Based on a Dynamic Corner Frequency, Bulletin of the Seismological Society of America, 95, no. 3, 995–1010, doi: 10.1785/0120030207.

Oth, A., D. Bindi, S. Parolai, and D. Di Giacomo, 2011, Spectral Analysis of K-NET and KiK-net Data in Japan, Part II: On Attenuation Characteristics, Source Spectra, and Site Response of Borehole and Surface Stations, Bulletin of the Seismological Society of America, 101, no. 2, 667–687, doi: 10.1785/0120100135.

Oth, A., D. Bindi, S. Parolai, and D. Di Giacomo, 2011, Spectral Analysis of K-NET and KiK-net Data in Japan, Part II: On Attenuation Characteristics, Source Spectra, and Site Response of Borehole and Surface Stations, Bulletin of the Seismological Society of America, 101, no. 2, 667–687, doi: 10.1785/0120100135.

Parolai, S., D. Bindi, and P. Augliera, 2000, Application of the Generalized Inversion Technique (GIT) to a Microzonation Study: Numerical Simulations and Comparison with Different Site-Estimation Techniques, Bulletin of the Seismological Society of America, 90, no. 2, 286–297, doi: 10.1785/0119990041.

Parolai, S., D. Bindi, M. Baumbach, H. Grosser, C. Milkereit, S. Karakisa, and S. Zünbül, 2004, Comparison of Different Site Response Estimation Techniques Using Aftershocks of the 1999 Izmit Earthquake, Bulletin of the Seismological Society of America, 94, no. 3, 1096–1108, doi: 10.1785/0120030086.

Parolai, S., S. M. Richwalski, C. Milkereit, and P. Bormann, 2004, Assessment of the stability of H/V spectral ratios from ambient noise and comparison with earthquake data in the Cologne area (Germany), Tectonophysics, 390, no. 1, 57–73, doi: 10.1016/j.tecto.2004.03.024.

Pezeshk, S., A. Zandieh, and B. Tavakoli, 2011, Hybrid Empirical Ground-Motion Prediction Equations for Eastern North America Using NGA Models and Updated Seismological Parameters, Bulletin of the Seismological Society of America, 101, no. 4, 1859–1870, doi: 10.1785/0120100144.

Pilz, M., F. Cotton, R. Zaccarelli, and D. Bindi, 2019, Capturing Regional Variations of Hard-Rock Attenuation in Europe, Bulletin of the Seismological Society of America, 109, no. 4, 1401–1418, doi: 10.1785/0120190023.

Riccardo Zaccarelli, Dino Bindi, Angelo Strollo, Javier Quinteros, Fabrice Cotton; Stream2segment: An Open-Source Tool for Downloading, Processing, and Visualizing Massive Event-Based

Seismic Waveform Datasets. Seismological Research Letters 2019; 90 (5): 2028–2038. doi: https://doi.org/10.1785/0220180314

Zaccarelli, Riccardo (2018): Stream2segment: a tool to download, process and visualize event-based seismic waveform data. V. 2.7.3. GFZ Data Services.